The influence of 1,3-diaminopropane in functional groups generation on iron oxide nanoparticles surfaces synthesized by laser pyrolysis

A. D. BADOI[a], F. DUMITRACHE[a,b], C. T. FLEACA[a,b], N. MIHAILESCU[a], E. VASILE[c], C. LUCULESCU[a], L. GAVRILA[a], I. MORJAN[a], I. CIUCA[d]

[a]*National Institute for Laser Plasma and Radiation Physics, Laser Department Atomistilor 409, PO Box MG 36, RO-077125, Magurele, Romania*

[b]*"Politehnica" University of Bucharest, Physics Department, Splaiul Independentei 313, RO-060042, Bucharest, Romania*

[c]*"Politehnica" University of Bucharest, Faculty of Applied Chemistry and Material Science, Department of Oxide Materials and Nanomaterials, Gh. Polizu 17, RO-011061 Bucharest, Romania*

[d]*"Politehnica" University of Bucharest, Faculty of Materials Science and Engineering, Splaiul Independentei 313, RO-060042, Bucharest, Romania*

The synthesis of very fine maghemite-based nanoparticles (around 4 nm in size) using one step pulsed laser oxidative pyrolysis has been reported. In the synthesis of the first sample we used iron pentacarbonyl as precursor, air as oxydant and ethylene as laser energy transfer agent. The second sample was synthesized in similar conditions with supplementary introduction of 1,3-diaminopropane vapors in order to obtain a nitrogen-based functionalized nanoparticles surface. The samples were characterized by XRD, EDX, FTIR, TEM and SAED techniques which confirm the complex structure of the resulted nanoparticles with iron oxide cores surrounded by more disordered carbonaceous shells containing oxygenated and, for the second sample, nitrogenated functional groups.

(Received June 20, 2014; accepted February 10, 2016)

Keywords: Magnetic nanoparticle, Iron oxide nanoparticles, Laser pyrolysis, Diaminopropane

1. Introduction

Very fine iron oxide particles with dimensions less than 100 nm (usually named nanoparticles) and more specifically less than 10 nm attract a great interest for researchers from a wide range of applications, including magnetic fluids [1], catalysis [2], in-vivo and in-vitro biomedicine (as magnetic resonance imaging contrast enhancement, tissue repair, immunoassay, detoxification of biological fluids, drug delivery and in cell separation, etc) [3-7] and environmental remediation [8]**.** Moreover, other biomedical applications of iron oxide nanoparticles are widely studied including magnetically enhanced transfection [9], magnetically assisted gene therapy [10], magnetically induced hyperthermia [11, 12] and magnetic-force-based tissue engineering [13].

The conditions for obtaining nanoparticles can be chosen depending on the desired application by adapting the specific experimental synthesis parameters [14]. While a number of suitable methods have been developed for the synthesis of magnetic nanoparticles with various compositions, successful application of such magnetic nanoparticles in the areas listed above is highly dependent on their stability and dispersibility in application-specific fluids [15]. These requirements are mandatory both for industrial applications such as magnetic fluids or heat transfer nanofluids (where the iron oxide nanoparticles need to be dispersed in water or hydrophobic liquids) as well as for biological applications where the magnetic nanoparticles must to be introduced in the living organism as suspensions suitable for physiological fluids such as blood. For many of the listed applications, the nanoparticles must have a narrow particle size distribution and a very small size, therefore the most magnetic nanoparticles become superparamagnetic at room temperature [3, 16]. Also, two important features of magnetic nanoparticles should be highlighted: a high value for their magnetization saturation and a good chemical stability in base fluid in order to obtain a controllable delivery of theranostic agents [17].

The performant iron oxide nanoparticles production for biomedical applications must reach the following requirements: synthesis of large quantities of magnetic nanoparticles, narrow particle size distribution, tailored magnetic and structural properties and the presence of superficial functional groups to improve their stabilization/dispersion in physiological liquids. Particularly, for their biological and in vivo medical applications such as those that were mentioned before: drug delivery, tumor destruction by hyperthermia or enhanced MRI (Magnetic Resonance Imaging), the functionalized nanomaterials require biocompatible properties [14]. The amino functional group is a basic one and can be found in proteins, amino acids, nitrogenous

bases of DNA and RNA etc. and also can be used as a linker for further binding of various biomolecules [18] based on the formation of imino or amide bonds. There are several reports in literature concerning the coating of iron oxide nanoparticles with layers having nitrogen-containing groups such as: aminated silica from APTES (amino propyl triethoxysilane) [18], polyethyleneimine [19], or nitro substituted 3,4-dihydroxyphenylalanine (l-DOPA) derivates [20]. The introduction of amino groups via APTES or its analogue APTMS (aminopropyltrimethoxysilane) has as disadvantage the formation of a supplementary non-magnetic silica shell which diminishes the saturation magnetization of the functionalized nanoparticle.

The laser pyrolysis as powder production technique was initiated by Cannon and coworkers [21] since 1984. It is a versatile method, characterized by the use of vapor or gaseous precursors which require the presence of at least one compound (named sensitizer) that absorbs the infrared (IR) laser irradiation. This sensitizer (such as ethylene or sulfur hexafluoride) has the role to transform a part of the laser energy into thermal energy of the reactive species which decompose and further condense to form nanoparticles. Consequently, non absorbing precursors (in vapor or gas state) should be mixed with the sensitizer in order to generate proper conditions for laser induced decomposition. [22]. One advantage of this technique is the facile and external control of nanoparticles composition which can be achieved by tuning the process parameters (laser power, gas flows, pressure). Also, of major importance is the resulted narrow size distribution of particles due to a fine control of reaction zone and the coresponding residence time. Moreover, it is a continuous method with the potential to be scaled up to industrial applications. Iron oxide nanoparticles synthesized by laser pyrolysis should have spherical shape, precise dimension, superparamagnetic properties and relatively high saturation magnetization [23].

In this work, a comparative study on the synthesis and characterization of iron oxide nanoparticles with or without nitrogen-containing groups on the surfaces has been performed. The effect of 1,3-diaminopropane (DAP) vapors addition into an oxidative mixture (air, iron pentacarbonyl vapors, ethylene) has been studied by comparing the differences in elemental composition, crystallinity, infrared absorption bands and mean particle size distributions between the above mentioned samples. It is worth noting that Fe-based nanoparticles with other modified surfaces has been previously synthesized using laser pyrolysis by our group [24, 25]. In those studies, organosiloxane or methyl methacrylate were used as additives and TEM investigations revealed nanoparticles with composite structure: Fe/Fe_2O_3 nano cores enveloped in different polymeric shells. In our new approach, we functionalized the iron oxide surfaces with nitro groups which can be reduced to amino without the formation of a silica shell.

2. Experimental

Laser pyrolysis experimental set-up is presented in Fig. 1. A focused (at 4 mm above the injector) pulsed CO_2 laser radiation (Diamond G-series laser from Coherent INC. - 70 W maximum output power, λ=10.6 μm, frequency 200 kHz, filling factor 50 %) crossed orthogonally the reactive gas flows. The $Fe(CO)_5$ (iron precursor) vapors entrained by an argon flow encounter the diaminopropane vapors carried by the ethylene sensitizer flow via two different bubbler systems. Also, an air flow was added through the inner nozzle of the injector together with previous mixture (as presented in Fig. 1). The resulted sample was labeled SFP6. In the second case, the gas mixture which contained only air, $Fe(CO)_5$ vapors entrained by Ar and C_2H_4 was used to synthesize the SFP1 undoped sample (no N surface addition). The confinement of the reactive gases and of the synthesis products was achieved by a coaxial argon flow admitted through the outer tube (the same values in both experiments: 2000 sccm). In order to prevent the ZnSe windows from being contamined with powder they were continuously flushed with Ar. In both experiments, the following parameters were maintained constant: ethylene flow: 100 sccm, Ar flow through $Fe(CO)_5$: 50 sccm, air flow: 50 sccm, laser power: 67 (± 3) W and the nozzles system (the inner nozzle diameter has 3.1 mm).

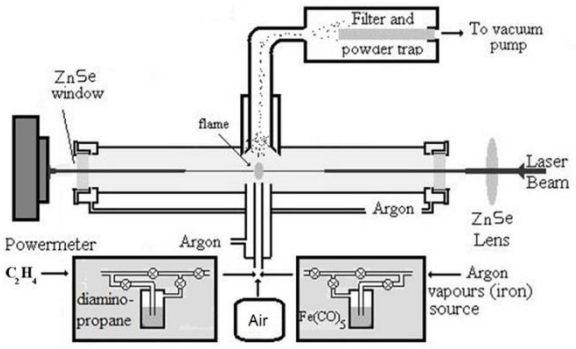

Fig. 1. Experimental set-up for obtaining nanometric iron oxides

The elemental composition of both samples was evaluated using a Energy-dispersive X-ray spectroscopy (EDX), using an EDAX Co. SiLi detector mounted inside Scanning Electron Microscope (SEM), FEI Co., model Quanta Inspect S, 0–30 kV accelerating voltage. The morphology and composition of the iron oxides nanopowders were characterized with a Tecnai F30 G2 (300 kV) Transmission Electron Microscope (TEM) which can provide also selected area electron diffraction (SAED) analysis. X-ray diffraction (XRD) measurements were performed on a PANalytical X'Pert PRO MPD X-ray diffractometer (Cu Kα wavelength). The crystallite sizes were evaluated applying the Scherrer formula to the instrumental corrected full width at half maximum

(FWHM) of selected peaks. The FWHM value was extracted from the fitted peak profile using pseudo-Voigt function. For infrared IR analysis, a Shimadzu 8400S Fourier Transform Infrared (FTIR) Spectroscope was used.

3. Results and discussion

The XRD diffractograms point out the presence of a major crystalline phase $\gamma Fe_2O_3/Fe_3O_4$ with a minor contribution from α-Fe phase (see Fig. 2), especially for SFP1 sample (synthesized without nitrogen-containing precursor). The mean crystalline sizes (d_{mean}) were evaluated from the FWHM of (440) peak: 4.0 nm for SFP1 and 4.3 nm for SFP6.

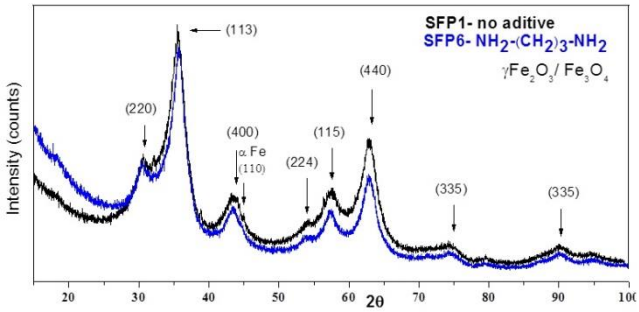

Fig. 2. The superposed X-ray diffractograms of the powders obtained in the two experiments

The elemental composition extracted from EDX spectra are presented in Table 1. The elemental analysis of both samples show that O/Fe atomic ratio is higher than that corresponding to the stoichiometric Fe_2O_3 (O/ Fe= 1.5). The oxygen excess can be explained be its presence in functional groups at the surface of iron oxide nanocrystals (-COOH, -NO, NO_2 etc). Also, the presence of carbon provided by ethylene or carbon monoxide (from $Fe(CO)_5$ decomposition) points out the oxygen-deficient environment in our laser pyrolysis experiments. Thus, an explanation of this carbon and also traces of metallic iron presence might be an incomplete oxidation of $Fe(CO)_5$ and C_2H_4. The successful incorporation of the nitrogen from DAP in the SFP6 sample is confirmed by EDS analysis.

Table 1. EDX elemental estimation

Sample	aditive	C (at.%)	O (at.%)	Fe (at.%)	N (at.%)
SFP1	-	15.4	53.4	31.2	-
SFP6	$NH_2(CH_2)_3NH_2$	19.6	47.3	26.6	6.5

The IR peaks of maghemite were observed in both samples in the 409-640 cm^{-1} zone (see Fig. 6), similar with those reported by Veintemillas et al. in [26]. Also, the IR signature of C=C and C=O bonds can be identified in both powders (see Fig. 3). This can be related with the presence of carbon in our samples (detected at EDX) confirming the hypothesis of an oxygen-deficient in the flame. The FT-IR analysis revealed new absorption bands from some N-based functional groups with different oxidation degrees (such as nitro and nitroso) in the case of sample SFP6. Their presence can be explained by the catalytic decomposition of DAP in the presence of freshly formed iron based clusters, ethylene and oxygen molecules.

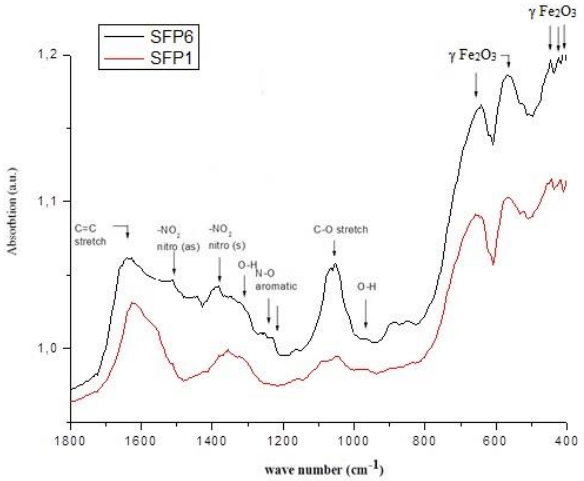

Fig. 3. FTIR spectra of the two oxide samples

Low resolution TEM images (Fig. 4 a, b) reveal aggregated nanoparticles, most of them having a spherical shape and being surrounded by an almost uniform and close-packed grey layer, most evident for sample SFP6. HRTEM image from SFP1 sample (Fig. 4 c) shows an encapsulated particle where the crystalline core has lattice plane fringes belonging to γFe_2O_3 (311) planes - 2.5 Å. The small size of our maghemite-based nanoparticles (around 4-6 nm) is close to the mean crystalline diameter extracted from X-ray diffractograms, indicating the presence of the single-crystalline particles. The iron oxide cores have an amorphous organic/polymeric shell, visible also in the HRTEM image (Fig. 4 d) from sample SPF6 where turbostratic/distorted graphene-like layers can be also observed. The observation of the less structured/disordered layers that surround the maghemite nanoparticles are correlated with the IR spectra where different C=C, C/O (for SFP1) and C/N/O groups (for SFP6) has been identified.

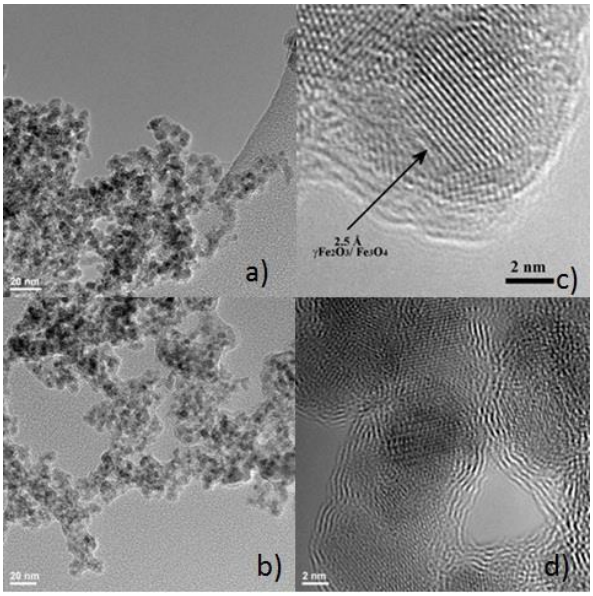

Fig. 4. TEM images of (a) SFP1 and (b) SFP6 and HRTEM images of: (c) SFP1 and (d) SFP6 nanopowders

The SAED analyses confirm the presence of maghemite/magnetite phases found in the X-ray diffractograms of both samples. The rings which correspond to the crystalline planes of these phases are identified in the Fig. 5. Also, the appearance of these broad diffraction rings together with the diffraction spots can be related with the existence of very small crystallites with some lattice defects.

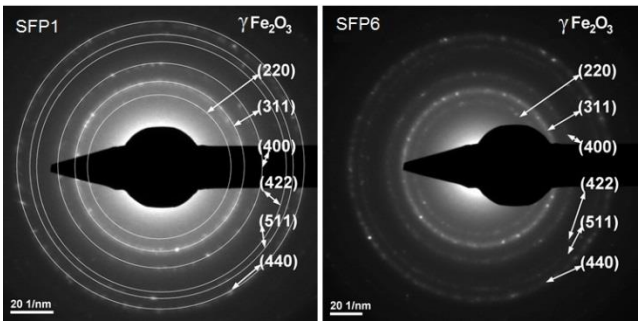

Fig. 5. SAED images from the SFP1 and SFP6 samples

Corroborating the all characterization techniques mentioned before we can conclude that the resulted nanopowders are composed from maghemite/magnetite nanoparticles covered with the carbonaceous layer rich in oxygenated/nitrogen-containing groups.

The presence of the nitro groups (identified the IR Spectroscopy and originated from the oxidation of the amino groups from the organic precursors) on the surfaces of iron oxide based nanoparticles can open the path for their further functionalization with various biological molecules or labelling agents. This approach is based on the hydrogenation of NO_2 groups to NH_2 followed by coupling with glutaraldehyde in a similar way with the APTMS or APTES coupled magnetic nanoparticles [27]. This process can be represented as following:

$$\text{Nanoparticle-NO}_2 + \text{H}_2 \rightarrow \text{Nanoparticle-NH}_2 + \text{H}_2\text{O}$$
$$\text{Nanoparticle-NH}_2 + \text{O=CH-(CH}_2)_3\text{-CH=O} \rightarrow \text{Nanoparticle-N=CH-(CH}_2)_3\text{-CH=O} + \text{H}_2\text{O}$$

The resulted functionalized nanoparticles with aldehyde groups can be further coupled with amino groups from various biomolecules such as: amino acids, peptides, proteins/enzymes [28] or biocompatible polymers like chitosan [29]. Moreover, the surface amino groups can be directly coupled with fluorescent dye such as FITC (fluorescein isothiocyanate) in a similar way with silica APTES-nanoparticle reported in [30], resulting magnetic-fluorescent iron oxides nanoparticles suitable for cells labelling.

4. Conclusion

Laser pyrolysis was successfully employed for synthesis of very small iron oxide based nanoparticles. XRD, FTIR, SAED and HRTEM analysis reveal a major content of maghemite/magnetite in both samples. Those nanoparticles are organized as loosely agglomerated/aggregated structures. The mean particle size was found to be around 4 nm according to TEM and XRD analysis. The nanoparticles from both samples are covered with a carbonaceous shell rich in oxygenated groups (as revealed by EDX and FTIR). When the DAP was introduced in the reactive mixture the resulted nanoparticles shells contains also nitrogen and oxygen-based groups. The primary functionalization of these nanoparticles surface can open the way for the attachment of other complex molecules resulting thus performant nanosystems with potential applications in biomedicine. Regarding our specific nanoparticles, the nitro groups found on the surface can be reduced to the amino groups which can be coupled for example with glutaraldehyde and as linker for peptides, proteins or biocompatible polymers like chitosan or directed coupled with fluorescent dyes such as FITC.

Acknowledgement

This work was supported by Romanian Ministry of Education, through the Project **PN 09390101** and by the Sectoral OperationalProgramme Human Resources Development 2007–2013 of the Ministry of European Funds through the Financial Agreement POS-DRU/159/1.5/S/134398.

References

[1] S. Chikazumi, S. Taketomi, M. Ukita, M. Mizukami, H. Miyajima, M. Setogawa, Y. Kurihara, J. Magn. Magn. Mater. **65,** 245 (1987).

[2] M. Shokouhimehr, Y. Piao, J. Kim, Y. Jang, T. Hyeon, Angew. Chem. Int. Ed. **46**, 7039 (2007).

[3] A. K. Gupta, M. Gupta, Biomaterials **26**, 3995 (2005).

[4] S. Mornet, S. Vasseur, F. Grasset, P. Verveka, G. Goglio, A. Demourgues, J. Portier, E. Pollert, E. Duguet, Prog. Solid State Chem. **34**, 237 (2006).

[5] Z. Li, L. Wei, M. Y. Gao, H. Lei, Adv. Mater. **17**, 1001 (2005).

[6] O. Veiseh, J. Gunn, M. Zhang, Adv Drug Deliv Rev. **62**, 284 (2010).

[7] J. Safari, Z. Zarnegar, Journal of Saudi Chem Society **18**, 85 (2014).

[8] M. Takafuji, S. Ide, H. Ihara, Z. Xu, Chem. Mater. **16**, 1977 (2004).

[9] C. F. Adams, M. R. Pickard, D. M. Chari, Nanomed: Nanotech, Biology, and Medicine **9,** 737 (2013).

[10] C. Li, L. Li, A. C. Keates, Oncotarget **3**, 365 (2012).

[11] F. Sonvico, S. Mornet, S. Vasseur, C. Dubernet, D. Jaillard, J. Degrouard, J. Hoebeke, E. Duguet, P. Colombo, P. Couvreur, Bioconjugate Chem. **16**, 1181 (2005).

[12] C. S. S. R. Kumar, F. Mohammad, Adv Drug Deliv Rev **63,** 789 (2011).

[13] J. Corchero, A. Villaverde, Trends Biotechnol **27**, 468 (2009).

[14] S. Naahidi, M. Jafari, F. Edalat, K. Raymond, A. Khademhosseini, P. Chen, Journal of Controlled Release **166**, 182 (2013).

[15] A. Lu, E. L. Salabas, F. Schuth, Angew. Chem. Int. Ed. **46**, 1222 (2007).

[16] G. S. Alvarez, M. Muhammed, A. A. Zagorodni, Chemical Engineering Science **61**, 4625 (2006).

[17] D. Yoo, J. H. Lee, J. H. Shin, J. Cheon, Accounts of Chemical Research, **44**, 863 (2011).

[18] B. K. Sodipo, A. A. Aziz Beilstein J. Nanotechnol. **5**, 1472 (2014).

[19] X. Wang, L. Zhou, Y. Ma, X. Li, H. Gu, Nano Res **2**, 365 (2009).

[20] E. Amstad, T. Gillch, I. Bilecka, M. Textore, E. Reimhult, Nano Lett. **9**, 4042 (2009).

[21] W. R. Cannon, S. C. Danforth, J. H. Flint, J. S. Haggerty, R. A. Marra, Journal of the American Ceramic Society **65,** 324 (1982).

[22] R. Alexandrescu, I. Morjan, F. Dumitrache, M. Scarisoreanu, C. T. Fleaca, I. P. Morjan, A. D. Barbut, R. Birjega, G. Prodan, App. Surf. Science **278**, 305 (2013).

[23] M. P. Morales, O. Bomati-Miguel, R. Pérez de Alejo, J. Ruiz-Cabellob, S. Veintemillas-Verdaguera, K. O'Gradyc, J. Magn. Magn. Mater. **266**, 102 (2003).

[24] A. Galykova, Z. Bastl, R. Alexandrescu, I. Morjan, J. Pola, Thermochimica Acta **439,** 80 (2005).

[25] R. Alexandrescu, I. Morjan, A. Tomescu, C.E. Simion, M. Scarisoreanu, R. Birjega, C. Fleaca, L. Gavrila, I. Soare, F. Dumitrache, G. Prodan, Journal of Nanomaterials Art. ID 324532 (2010).

[26] S. Veintemillas-Vertaguer, M. P. Morales, C. J. Serna, Appl.Organomet.Chem. **15**, 365 (2001).

[27] I. Koh, X. Wang, B. Varughese, L. Isaacs, S. H. Ehrman, D.S. English, J. Phys. Chem. **B 110**, 1553 (2006).

[28] S. Y. Shaw, Y. J. Chen, J. J. Ou, L. Ho, Enzyme and Microbial Technology **39**, 1089 (2006).

[29] V. Kumar, F. Jahan, S. Raghuwanshi, R. V. Mahajan, R. Kumar Saxena, Biotechnology and Bioprocess Engineering **18**, 787 (2013).

[30] A. Blaaderen, A. Vrij, Langmuir **8**, 2921 (1992).

*Corresponding author: anca.badoi@inflpr.ro